ISSN 2070-2051, Protection of Metals and Physical Chemistry of Surfaces, 2020, Vol. 56, No. 2, pp. 302–310. © Pleiades Publishing, Ltd., 2020.

NANOSCALE AND NANOSTRUCTURED MATERIALS AND COATINGS

Insight into Oxidation of Lead Powder during Electrodeposition

Chang-jiang Yang[a], *, Lv-xing Zhao[a], Xu Zhang[a], Da-cheng Zhai[a], and Yu Gu[a]

[a] *Faculty of Metallurgical and Energy Engineering, Kunming University of Science and Technology, Kunming, 650093 P.R. China*

**e-mail: chemdut@163.com*

Received September 26, 2019; revised October 20, 2019; accepted October 29, 2019

Abstract—Pure lead powder can be electrodeposited by reduction of lead ions (Pb^{2+}) in aqueous electrolyte. In this investigation, ultra-fine lead powders with a minimum median diameter of 4.5 μm were electrodeposited in acetate solution. The formation mechanism of lead oxide (PbO) during electrodeposition was proposed. Operation parameters such as pH value, current density, and gelatin had remarkable influence on oxidation degree, median diameter, and current efficiency, which were detailed for the first time. Metallic Pb was formed with strong (111) preferred orientation, and micrography, composition, and structure were characterized. Amorphous PbO was found in as-deposited lead powder, and a gel-layer process was proposed to elucidate the formation of PbO. It was suggested the Pb···OH was the most important intermediate state to form PbO and the gel-layer played the key role in generation of pure lead powder.

Keywords: lead powder, oxidation, electrodeposition, mechanism

DOI: 10.1134/S2070205120020306

1. INTRODUCTION

Pure lead powder has extensive applications such as oil and gas exploration, X-ray shield, golf club manufacture, paints, lubricating grease and anti-friction products [1]. Recently, ultra-fine or nanoscale lead powders have attracted considerable attention as a superconductor [2], electronic materials, electrochromic materials [3], etc. Many methods [4, 5] to produce lead powder have been developed including casting, mechanic commuting, chemical reaction and liquid metal atomization, etc. Melt Atomization method has been commercially used to produce lead powders owing to high production rates and low cost [6, 7]. The air atomized Pb powders are usually semi-spherical shape with the average grain sizes in the range of 45 to 500 μm [7]. Chemical reduction and electrochemical deposition are well-suited to prepare lead powder with controllable size since its desirable feature of easy control of operation parameters, as well as low capital investment and operational costs [8].

Nanoscale lead powder can be directly prepared using different reducing agents. Wang et al [9] have reported lead nanowire with an average diameter of 80 nm was fabricated on the zinc foil via galvanic displacement method in lead acetate aqueous solutions. Rabah [10] prepared lead powder with mean particle diameters in the range of 90–120 nm by hydrazine hydrate and ascorbic acid. Thermal decomposition was also reported to obtain lead powder. Varavko et al. [11] prepared lead particles in a narrow size range (from 0.2 to 0.8 μm) by mixed oleic acid alkylolamide with lead formatted and heated to 240°C. Wang et al [12] synthesized Pb nanowires with uniform diameters in the range 50–90 nm using mixture of lead acetate and poly-(vinyl pyrrolidone) (PVP) in ethylene glycol.

Electrodeposition is a common method to fabricate lead powder with low energy consumption from the acid electrolytes based on fluoroborate [13], acetate [14, 15], borate [16], nitrate [2, 17], halides [18, 19], perchlorate [20–22], etc., an alkaline solution [5, 23, 24], and ionic liquid [25, 26]. The as-obtained lead powder by such techniques usually has extremely high surface area, which favors the use as electrodes in electrochemical devices [2, 13]. Moreover, lead powder obtained by electrodeposition is easily pressed and sintered due to irregular morphological forms of crystals and dendrites [27, 28]. Nikolić et al. [8, 29, 30] have investigated the morphologies and mechanisms of Pb powder obtained by electrolysis of aqueous nitrate, acetate, and alkaline electrolytes. Morphologies of lead powder depended on the type of electrodeposition control and showed cobweb-like or spongy-like in the dilute electrolytes while needle-like or fern-like dendrites in the concentrated electrolytes. Nikolic [27] proposed the lead electrodeposition mechanism which was either mixed ohmic-diffusion or completely ohmic controlled depending on the concentration of Pb(II) ions. The influence of additive on Pb microstructures was also examined, e.g., glycerol [5, 24], cetyltrimethylammonium bromide, sodium dodecyl benzene sulfonate, tartaric acid [31], sorbitol [32], Cu^{2+} [3], etc.

It is well known that Pb can be applied as corrosion protection on steel alloys in industrial atmospheres. Nevertheless, oxidation of lead powder during electrodepositing process is crucial for application, such as sintering [33], which actually decreased the purity and quality of lead powders compared to atomized ones. Owais [19] found lead oxides in the deposited Pb powders, which was explained with surface oxidation of the powders during the drying step. Actually, Sun et al. [34] and Lü [35] reported the cathodic synthesis of PbO in lead nitrate aqueous solution. In the deaerated acetate electrolyte, PbO in the lead deposit was determined by X-ray diffraction analysis (XRD) even in the high acid solution. Ghali and Girgis attributed the formation of PbO to a change of pH around the cathode and atmospheric oxygen [14]. Zhitomirsky et al. [36] and Macpherson et al. [37] elucidated the mechanism of the cathodic deposition of PbO from an aqueous solution of $Pb(NO_3)_2$ was due to the interaction of Pb^{2+} cations with OH^- ions arising from electrochemical reduction of nitrate ions as the following process:

$$O_2(aq) + 2H_2O + 4e^- \rightarrow 4OH^-(aq), \quad (1)$$

$$NO_3^-(aq) + 7H_2O + 8e^- \rightarrow NH_4^+(aq) + 10OH^-(aq), \quad (2)$$

$$Pb(OH)_2 + OH^-(aq) \rightarrow Pb(OH)_2, \quad (3)$$

$$Pb(OH)_2 \rightarrow PbO(s) + H_2O. \quad (4)$$

However, Sawatani et al. [38] concluded that freshly deposited metallic Pb was oxidized and converted into PbO under oxygen, and OH^- ions generated by electroreduction of NO_3^- and/or O_2 had no contribution to the formation of PbO. Kwon [39] hold the same opinion that electrodeposited Pb particles were autonomously converted to PbO nanostructures in the oxygen contacting aqueous media. Such was supported by Cheng's work [40], in which only metallic Pb was electrodeposited, and no PbO directly precipitated in parallel with Pb deposition.

It should be noted that up to now, the formation of PbO during electrodeposition of lead powder was still unclear and the reported mechanism was controversial. The insight into the oxidation process played a crucial role in cathodic production of both high-pure Pb or PbO powder. In this work, new light was thrown on the oxidation mechanism of lead powder during the electrodeposition in acetate solution as a function of pH, current density, and organic additive.

2. EXPERIMENTAL

2.1. Chemicals and Materials

Sodium acetate (CH_3COONa), ammonium acetate (CH_3COONH_4), lead(II) acetate trihydrate ($Pb(CH_3COO)_2\,3H_2O$), glacial acetic acid (CH_3COOH), sodium hydroxide (NaOH), gelation, ethylenediamine tetraacetic acid disodium salt dihydrate (EDTA), hexamethylene tetramine (HMTA), absolute ethanol (CH_3CH_2OH), ammonium hydroxide solution (NH_4OH, 25.0–28.0% NH_3 basis), and xylenol orange tetrasodium salt (XO) were of analytical grade and purchased from Sinopharm Chemical Reagent Co. Ltd. Lead foils (99+%) and titanium foils (99.2%) were purchased from Alfa Aesar. Unless otherwise stated, the reagents were used as received without further treatment. Pure water (specific resistance 18 MΩ cm) was used for the preparation of aqueous solutions.

2.2. Synthesis of Lead Powder

Galvanostatic electrodeposition of lead powder was carried out by a linear DC power supply (GPD-2303S, GW Instek) in lead acetate solution containing 0.002 mol L^{-1} $Pb(CH_3COO)_2$ and 2 mol L^{-1} CH_3COONa. The pH value of the electrolyte was adjusted by CH_3COOH or NaOH, i.e., ~84 mL L^{-1} CH_3COOH was added to obtain a solution at neutral pH. At the beginning of electrolysis, an UltraBasic pH Meter (UB-7, Denver) was used to determine the pH values. Titanium foil and lead foil were used as the working electrode and auxiliary electrode, respectively. All electrodes were polished with wet abrasive papers grade by grade to 2000 grit sandpaper, and then ultrasonically cleaned with ethanol and acetone. The polished samples were tested immediately. As-deposited lead powder was scraped away on the surface of titanium cathode by a blade at the interval of 15 min. Immediately, the powder was washed and filtered thoroughly with absolute ethanol. The final lead powder was obtained by drying the solid in vacuum oven at 60°C for 4 h and kept in desiccator prior to analysis.

2.3. Measurement of Oxidation Degree

The content of PbO in the lead powder was determined by a complexometric titration with EDTA [41, 42]. Briefly, about 0.5 g as-synthesized lead powder was added to 20 mL 5% acetic acid in an Erlenmeyer flask to dissolve PbO. Then, 80 mL water, 10 mL acetic acid-ammonium acetate buffering solution (pH 5), and 5 mL 20% HMTA were sequentially added under stirring. Subsequently, a little 10% ammonium hydroxide solution was used to increase the pH value to 5.5. The final solution was titrated by a standard EDTA solution (0.05 mol L^{-1}) with 3 drops of 0.2% XO as the indicator. The oxidation degree (OD, %) was calculated by the following equation:

$$OD(\%) = \frac{207 \times W_{PbO}}{W_T - 16 \times W_{PbO}} \times 100, \quad (5)$$

where, W_T is the total mass of lead powder in g, and W_{PbO} is the molar mass of PbO from the above titration in mol.

2.4. Characterization of Materials

The morphology of the lead powder was acquired using electron probe microanalyzer with scanning electron microscopy (SEM, EMPA-1720, Shimadzu), and field-emission transmission electron microscopy (Nova Nano SEM 450, FEI). The atomic structure was conducted by scanning transmission electron microscope (STEM) and high-resolution transmission electron microscope (HRTEM, Tecanai G^2 TF30, FEI). X-ray diffraction (XRD, D/Max 2200, Rigaku) using a CuK_α (1.54056A) target was carried out with a scanning rate of 8°/min with a step of 0.02°. The elements of lead powder were recorded by X-ray photoelectron spectroscopy (XPS, PHI5000Versaprobe, Ulva-phi). The particle size distributions and median diameters of lead powder were processed by a laser diffraction particle size analyzer (Winner2000, WEINA).

3. RESULTS

3.1. Effect of pH Values

Lead powder was electrodeposited under current density of 2.3 A dm^{-2} in the electrolyte solution with pH value of 1, 3, 5 and 7, respectively. The current efficiency was calculated by the ratio of the actual mass of as-synthesized lead powder to the theoretical mass according to Faraday's law. Figure 1 shows the particle size distribution of lead powder in all pH values and the oxidation degree, median diameter, and current efficiency as a function of pH value. The particle sizes of lead powder formed in all pH values are less than 30 μm. Two peaks at ~0.7 μm and ~10 μm in the particle size distribution curves (Fig. 1a) probably resulted from the initial emergence of lead crystal nucleation and progressive growth of lead dendrite respectively. This was in well agreement with the mechanism proposed by Nikolić et al. [17, 27, 29]. The oxidation degree had the similar trend shape to D_{50}, which should be the first time observed to the best of our knowledge. The oxidation degree of lead powder reached to ~16% when pH value of electrolyte was 1 and decreased abruptly to ~6% at pH value from 3 to 7. During the electrodeposition of lead on cathode, intense bubbles emerged, indicating the parallel side reactions of evolving of hydrogen (HER) [24]. When the pH value was 1, the cathodic reaction favors HER in consequence of an abundance of proton, resulting in lower current efficiency. While pH > 5, the current efficiency increased significantly, which should be attributed to the predominant complex ions of Pb transferring from $[Pb(H_2O)^{2+}]$ to $[PbOH^+]$ [43] and the later should be much faster to be reduced. When

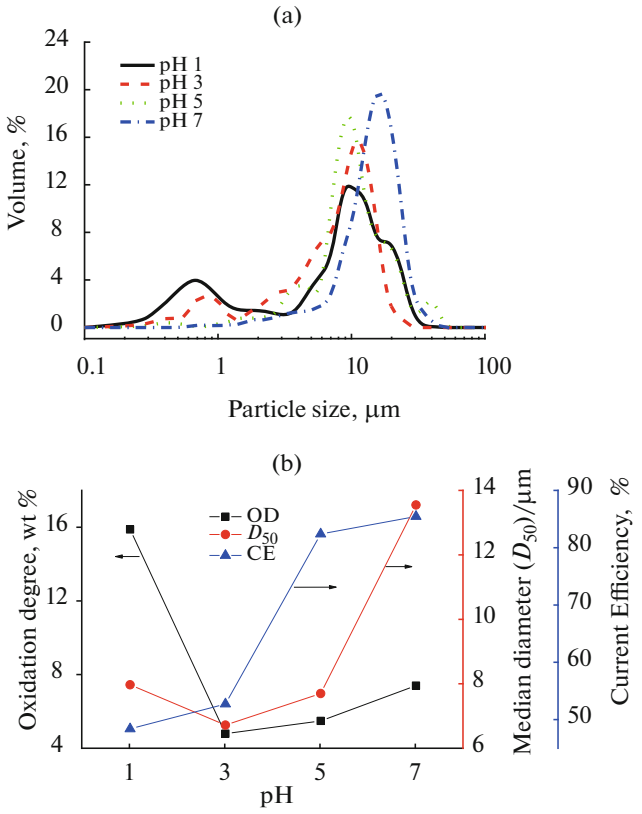

Fig. 1. (a) Particle size distribution of lead powder formed in electrolyte with pH value of 1, 3, 5 and 7; (b) The oxidation degree, median diameter and current efficiency as a function of pH value.

pH value of the electrolyte reaches natural, polynuclear complexes containing two or more lead atoms such as $\left[Pb_4(OH)_4^{4+}\right]$ and $\left[Pb_6(OH)_8^{4+}\right]$ were formed, which may accelerate the propagation of dendritic growth instead of formation of new nucleation, then leading to larger lead particle size.

3.2 Effect of Current Density

By keeping the pH value of the electrolyte solution at 3, the effect of current densities on the produced lead powder was explored. As shown in Fig. 2a, particle size distribution was similar to that of Fig. 1a. The oxidation degree of lead powder was stable at ~5% with the cathodic current densities at 2.3 and 3.6 A dm^{-2} and increased to 9 and 13% at current densities of 0.9 and 4.5 A dm^{-2} respectively. The curves of both oxidation degree and median diameter behaved U-shape, while the current efficiency showed an inverted V-shape. A large current density means a high cell potential and overpotential, and vice versa. Lead electrodeposition was ohmic control at low overpotential and ohmic-diffusion control at high overpotential. Whereas, HER in aqueous solution was kinetic control and boosted up with the increase of overpotential. Hence, as the

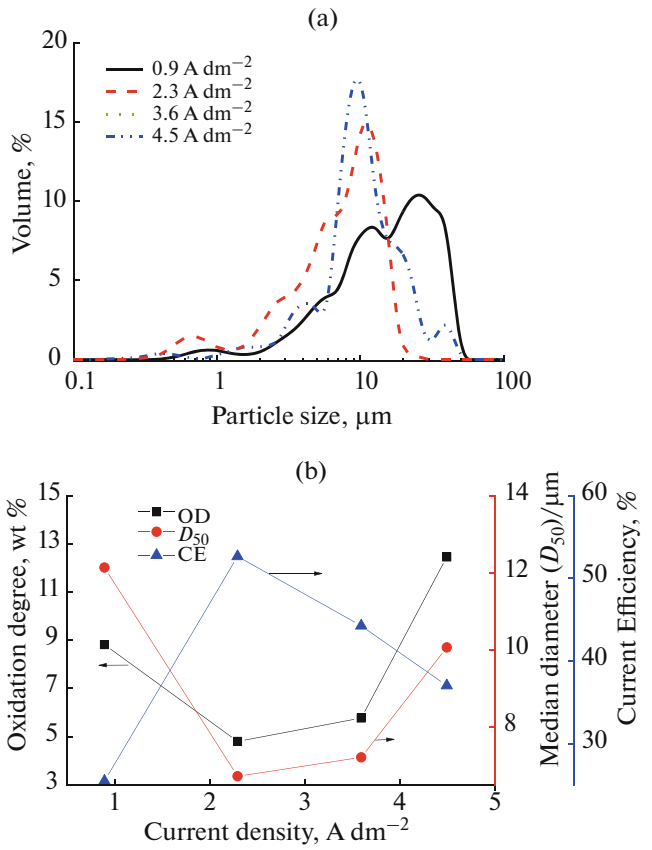

Fig. 2. (a) Particle size distribution of lead powder employing current density of 0.9, 2.3, 3.6 and 4.5 A dm^{-2} respectively; (b) The oxidation degree, median diameter and current efficiency as a function of current density.

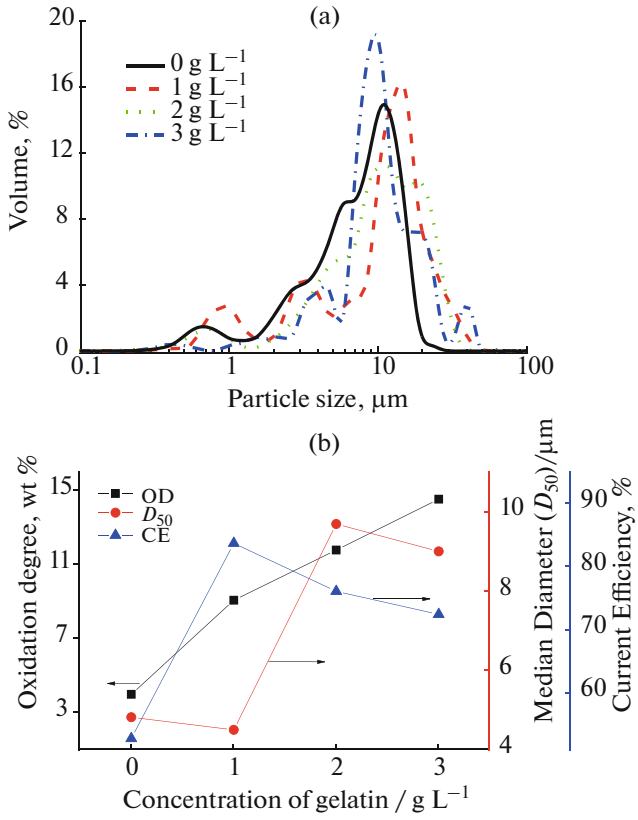

Fig. 3. (a) Particle size distribution of lead powder in the presence of gelatin of 1, 2 and 3 g L^{-2} respectively; (b) the oxidation degree, median diameter and current efficiency as a function of concentration of gelatin.

current density increased from 0.9 to 4.5 A dm^{-2}, the rate of lead depositing was ohmic control at first and much less than that of HER, and surpassed that of HER at current density of 2.3 A dm^{-2} due to a large exchange current density of Pb [44], then fell below that of HER owing to diffusion control. At low overpotential, the propagation of dendritic growth was prior to form new nucleation on titanium, and large particle formed [27]. The reason of large D_{50} at high overpotential was a consequence of the growth rate of the Pb crystal at the same time interval.

3.3. Effect of Gelatin

Gelatin has been widely used in metal electrodeposition. Therefore, gelatin as an additive was investigated with concentration of 1, 2 and 3 g L^{-2} under the condition of pH 3 and current density of 2.3 A dm^{-2}. Particle size distribution of lead powder in Fig. 3a was stable while compared to Figs. 1a, 2a. It was obvious that gelatin could suppress HER and improve the current efficiency. Nevertheless, lead deposition was also affected by high concentration of gelatin due to adsorption, which led to an inverted V-shape of current efficiency. The average diameter of lead power continuously increased with the addition of gelatin, indicating that the gelatin contributed to progressive growth of lead crystal [30]. The oxidation degree of lead powder increased approximately linear with the amount of gelatin added, and final reached a maximal value of ~15%.

3.4. Characterization of As-synthesized Lead Powder

Oxidation of lead powder was influenced by pH, current density and gelatin, and oxidation degree was highly related with median diameter of lead powder, i.e. a large diameter meant high oxidation degree. It was difficult to explain this phenomenon by the two mechanisms of ORR by Zhitomirsky et al. [36, 37] and/or oxidation of metal by Sawatani et al. [38–40]. Therefore, a further characterization of lead powder was important to elucidate oxidation of lead. Figure 4 presented the SEM images of lead particles obtained in the electrolyte with pH 7 for (a), 3 for (b) and 1 for (c), respectively. The micrographs are fern-like, rod-like, and needle-like, which were in well agreement with previous reports [23, 27, 30, 45] and our above analysis of diameters.

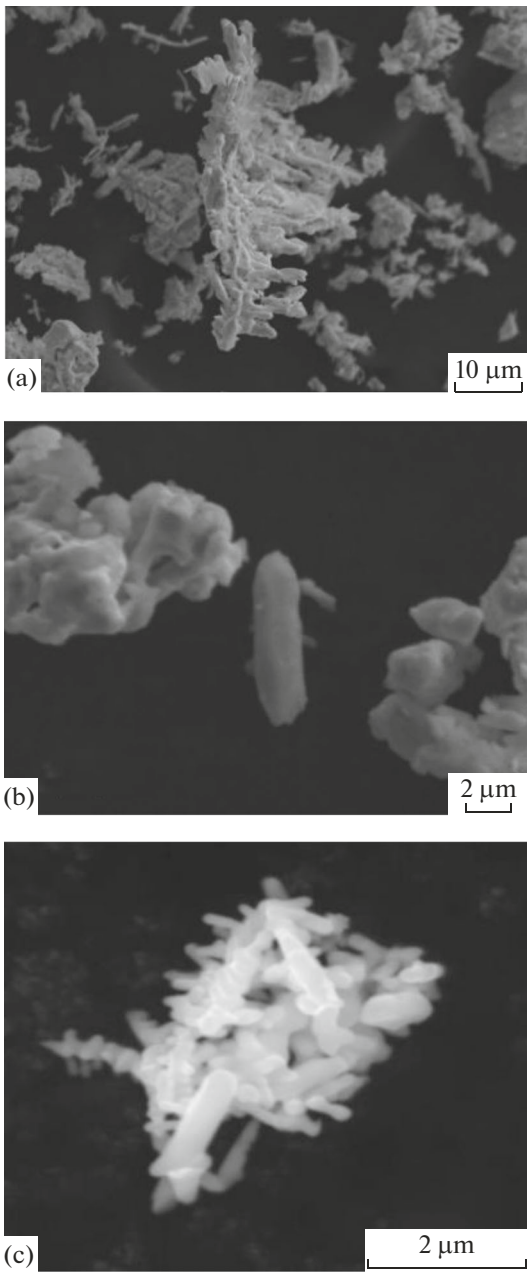

Fig. 4. SEM micrographs of lead particles obtained in the electrolyte with pH 7 for (a), 3 for (b) and 1 for (c).

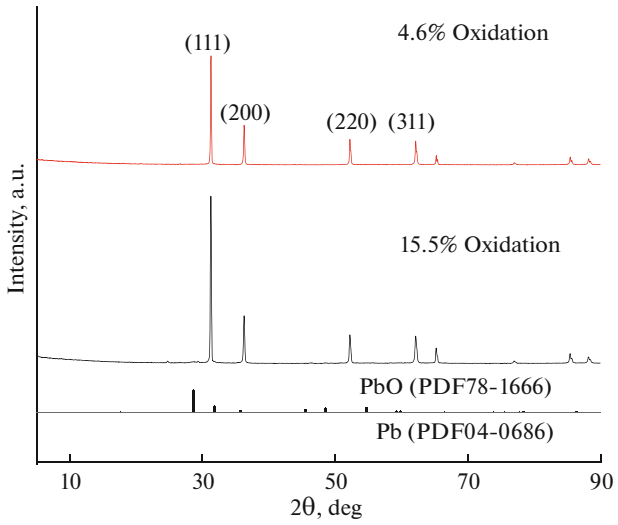

Fig. 5. XRD patterns of lead powders with oxidation degree of 4.6 and 15.5% respectively.

XRD patterns of lead powders with oxidation degree of 4.6 and 15.5% were shown in Fig. 5 respectively. XRD patterns were similar to each other with strong (111) preferred orientation. The peaks were close to the (111), (200), (220) and (311) of PDF card # 4-0686 that matched face-centered cubic of NaCl-type crystal structure. The XRD patterns of as-synthesized lead powder agreed remarkably well with the previous literatures [2, 23, 28]. It is interesting to note that no evidence of PbO reflections exists such as JCPDS card no. 78-1666 in Fig. 5. Cheng et al. [40] claimed that no peaks of PbO was observed in XRD of the Pb powder obtained in lead nitrate aqueous solution even containing 8.86% PbO. Ni et al. [31] found no PbO peaks in XRD in the presence of O in Pb powder via a galvanostatic method. It can be reasonable to conclude that lead oxide is formed as amorphous structure.

XPS was used to identify the elemental composition and bonding configuration on the surface of lead powder with 15% oxidation degree deposited in gelatin-added solution, as shown in Fig. 6. The distinctive features could be indexed to the characteristic's peaks of Pb 5d/4f/4d/4p, C 1s, S 2p, O 1s and N 1s. The presence of C 1s, S 2p and N 1s was attributed to absorption of gelatin on the surface of lead particles due to the capping effect. The deconvoluted Pb 4f core-levels high resolution XPS spectrum in Fig. 6b displayed the binding energies of the Pb $4f_{5/2}$ and Pb $4f_{7/2}$ peaks located at 143.45 and 138.59 eV with two satellite peaks located at 141.69 and 136.8 eV, respectively, which were characteristic of Pb^{2+} and Pb. The higher peak intensity of Pb–O bonds suggested the more content of PbO, as quantitatively estimated by the elemental analysis. The O 1s core-level high-resolution spectrum showed one intense peak and two shoulder peaks. These three peaks were fitted three Gaussian–Lorentzian curves and deconvoluted into 3 types of O species (Fig. 6c), which were likely attributed to the presence of Pb–O (529.3 eV), C–O– (531.3 eV), and –C=O (533.1 eV) bonds, respectively. The bonds between C and O were also supported by the peak centered at 286.6 and 288.6 eV of three distinct peaks in the C 1s core-levels spectrum respectively (Fig. 6d).

Further transmission electron microscopy (TEM) and high-resolution TEM (HRTEM) analysis mani-

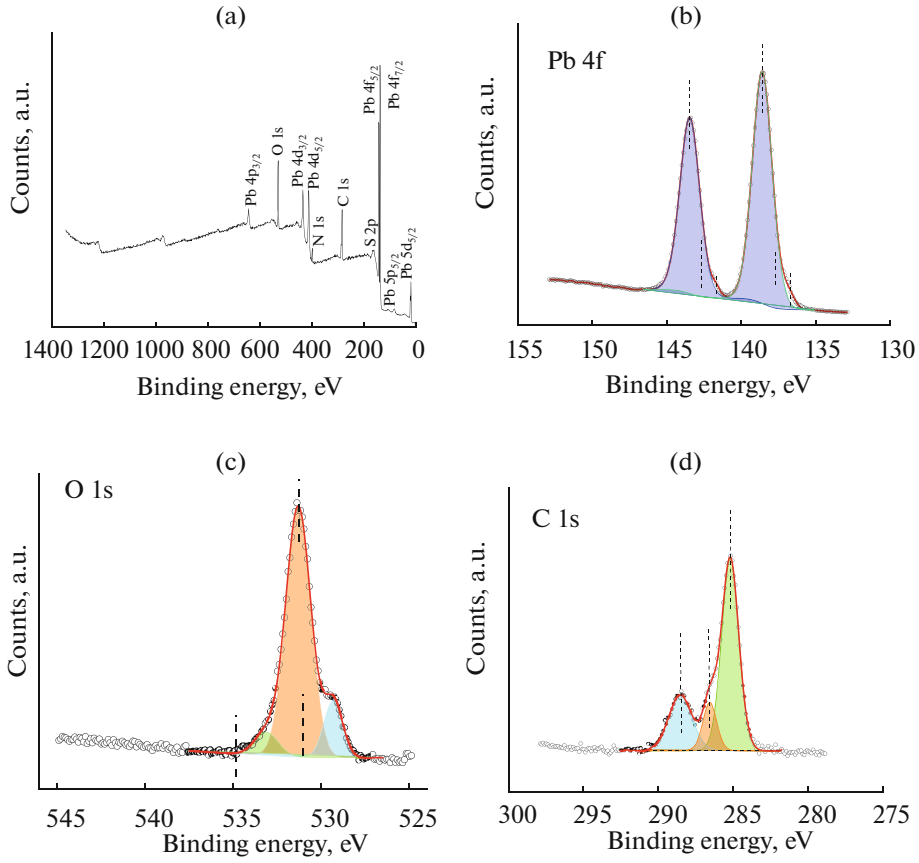

Fig. 6. XPS survey spectra of as-synthesized lead powder of 15% oxidation degree; (a) XPS survey spectrum; High-resolution XPS spectra deconvolution: (b) Pb 4f, (c) O 1s, and (d) C 1s core-levels.

fested the particle in Fig. 7. High-angle annular dark-field scanning transmission electron microscopy–energy-dispersive X-ray spectroscopy (HAADF–STEM–EDS) further confirmed that the particle was composed of Pb and O elements, and Cu and C elements were assigned to copper grids and carbon support film of TEM (as shown in Fig. 7c). The particle with a diameter of about 0.5 μm in Fig. 7a showed no diffraction spots and rings in selected area electron diffraction (SAD) patterns and no lattice fringe in HRTEM (insets in Fig. 7a), which was revealed as a completely amorphous PbO. A well-defined PbO polycrystalline core of the particle in insets of Fig. 7b was identified by the lattice fringe spacing matching well with the interplanar spacing corresponding to the (111) and (220) of PbO, which has been coated by a thick layer amorphous PbO layer.

4. DISCUSSIONS

Although there are two mechanisms of PbO formation including both cathodic alkalization Eqs. (1)–(4) and oxidation of fresh Pb particle, it is difficult to explain the correlation of oxidation degree with either average diameter or concentration of gelatin. Consequently, a new process of PbO formation was suggested with "gel-layer" intermediates and compatible with previous mechanisms, as shown in Fig. 8.

Polymer chains and gel structures on the surface of lead oxide were firstly proposed by Pavlov et al. [46–48]. Gel or hydrated or amorphous zones as the active center has both high electron and proton conductivities [48]. For the reduction of Pb ions, the gel-layer was predominated by Pb···OH, which depth was maintained through the dynamic equilibrium between the crystal and solution. The hydroxide layer on surface of Pb during electrodeposition was also proposed by Ehlers et al. [20] The calculation of DFT showed the Pb_2O was unstable and was decomposed as follows [49]:

$$Pb_2O \rightarrow PbO + Pb. \quad (6)$$

The reaction Eq. (6) was a disproportionation reaction with the Gibbs free energy of −107.6 kJ mol^{-1}. Nevertheless, Purkait et al. [50] obtained pure Pb_2O powder during Pb electrodeposition if dehydration of Pb···OH occurs under the control condition, which demonstrated existence of the gel layer.

Mechanism of cathodic alkalization as the reaction Eq. (1)–(4) was usually used to elucidate the formation of PbO in aerated solution. However, the solubil-

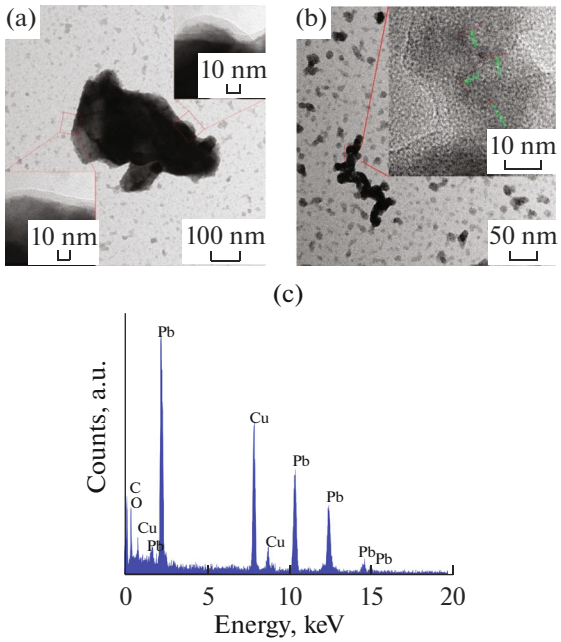

Fig. 7. TEM images of lead powder marked with boxes indicating selected region of interest for SAD and HRTEM (insets) (a) (b) and high-angle annular dark-field scanning transmission electron microscopy-energy-dispersive (c).

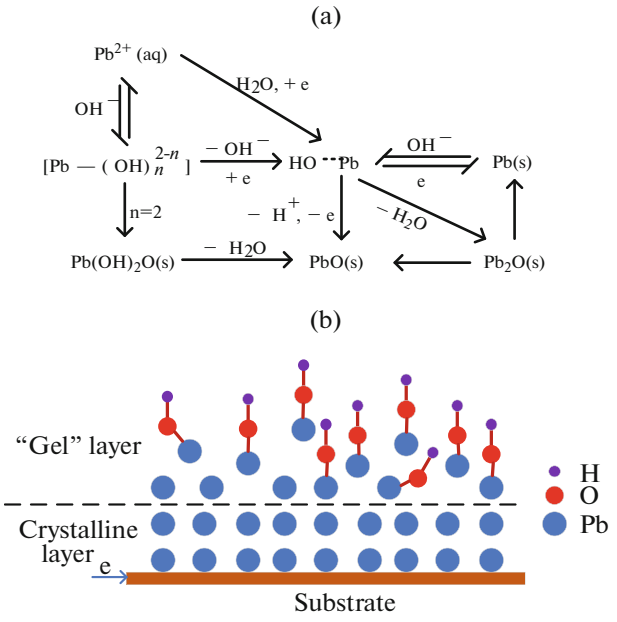

Fig. 8. (a) A process of Pb electrodeposition along with formation of PbO; (b) Structure of the gel-layer on the surface of Pb substrate.

ity of $Pb(OH)_2$ was minimum (~5 mg L^{-1}) at the pH value of 10–11 [43]. Hence, intense ORR and/or HER as side reaction were needed to form $Pb(OH)_2$ [51]. Moreover, dehydration of $Pb(OH)_2$ was usually at high alkali concentration and heated to 80–90°C [52]. In our case, gel-layer of Pb···OH was formed by cathodic reduction of $\left[Pb(OH)_n^{2-n}\right]$ (pH > 5) or $\left[Pb(H_2O)_n^{2+}\right]$ (pH < 5). ORR occurred on the gel-layer, and Pb···OH was oxidized to PbO.

While in the deaerated solution, Sawatani et al. [38, 39] proposed metallic Pb would be firstly electrodeposited and kept in "hot" state resulting in quickly oxidation to PbO by oxygen. After dried completely, the lead powder became inert like bulk Pb though it was open to water and oxygen for over a day [38]. Actually, the "hot" state of fresh lead powder was owing to gel-layer as active sites which could accelerate ORR and form galvanic cells with Pb substance until metallic Pb was totally transformed into PbO. At first, Pb was oxidized to Pb^+ ions and moved towards the gel-layer since the molar volume of PbO was larger by about 23% than that of Pb. Then, at the interface the Pb···OH reacted with oxygen to form PbO, which was in accordance with the growth/burst of PbO nanowires in various directions at the interface of water and oxygen with metallic Pb in the previous literature [39]. When the gel-layer was dried and dehydrated, Pb_2O formed and decomposed to PbO and Pb, which characters were just like bulk Pb. Since the gel-layer was amorphous, the PbO formed usually have the same structure, which was in good agreement with characters of XRD and TEM above.

The lead particle formed by electrodeposition were usually dendrites and the size of needle-like dendrites was larger than that of the fern-like dendrites [29]. In other words, both primary and secondary branches of large lead particles were not as big as the size of small particle [30]. Actually, relative quantity of the gel-layer of lead powder with big particle size was larger than that of the small one, leading to high oxidation degree of large particles. Surface adsorption of organic additive on lead powder was observed in many previous reports [14, 31]. As a hydrolyzed collagen, gelatin would enlarge the gel-layer instead of protecting lead powder from oxidation due to a gelling agent, which was confirmed by the XPS results. The stable chains between Pb_2O and R–COO– was reported previously [51]. Therefore, more gelatin in solution induced thicker gel layer and high oxidation degree.

5. CONCLUSIONS

Oxidation of lead during electrodeposition was investigated in acetate aqueous solution, which was out of view for several decades. We have for the first time explored the effect of several parameters on oxidation of lead including pH value, current density and gelatin. Low pH value of the electrolyte solution was helpful to obtain lead powder with higher oxidation degree, e.g. it reached to about ~16% for the electrolyte solution with pH value of 1, while decreased

abruptly to ~6% at pH from 3 to 7. The oxidation of lead powder was stable at ~5% with the cathodic current densities from 2.3 and 3.6 A dm^{-2} and increased to 9 and 13% at current densities of 0.9 and 4.5 A dm^{-2} respectively. The concentration of gelatin as an additive accelerated the oxidation degree of lead powder. More importantly, the average sizes of powder had a direct relationship with the degree of oxidation. Both XRD and TEM indicated the existence of amorphous PbO. We proposed a gel-layer process to elucidate the oxidation of lead, which suggested the Pb···OH as the most important intermediate state to form PbO or Pb during the cathodic reduction.

FUNDING

This work was financial supported by the National Natural Science Foundation of China (Project no. 51664040).

REFERENCES

1. Nikolić, N.D. and Popov, K.I., in *Electrodeposition and Surface Finishing*, Djokić, S.S., Ed., New York: Springer, 2014.
2. Yt, P., Gw, M., Ld, Z., Y, Q., Xy, G., Aw, Z., and Q, F., *Adv. Funct. Mater.,* 2002, vol. 12, p. 719.
3. Avellaneda, C.O., Napolitano, M.A., Kaibara, E.K., and Bulhões, L.O.S., *Electrochim. Acta,* 2005, vol. 50, p. 1317.
4. Chen, J.-H., Lo, S.-C., Chao, C.-G., and Liu, T.-F., *Jpn. J. Appl. Phys.,* 2008, vol. 47, p. 4815.
5. Wong, S.M. and Abrantes, L.M., *Electrochim. Acta,* 2005, vol. 51, p. 619.
6. Ashgriz, N., *Handbook of Atomization and Sprays,* Springer, 2011.
7. Ricks, R.A. and Clyne, T.W., *J. Mater. Sci. Lett.,* 1985, vol. 4, p. 814.
8. Nikolić, N.D., Stevanović, S.I., and Branković, G., *Trans. Nonferrous Met. Soc. China,* 2016, vol. 26, p. 3274.
9. Wang, C.-Y., Lu, M.-Y., Chen, H.-C., and Chen, L.-J., *J. Phys. Chem. C,* 2007, vol. 111, p.6215.
10. Rabah, M., *AIMS Mater. Sci.,* 2017, vol. 4, p. 1358.
11. Varavko, I.A., Radkevich, L.S., Chirkov, A.S., and Mironenko, N.N., *Sov. Powder Metall. Met. Ceram.,* 1990, vol. 29, p. 340.
12. Wang, Y., Jiang, X., Herricks, T., and Xia, Y., *J. Phys. Chem. B,* 2004, vol. 108, p. 8631.
13. Michotte, S., *Int. J. Mod. Phys. B,* 2003, vol. 17, p. 4601.
14. Ghali, E. and Girgis, M., *Metall. Trans. B,* 1985, vol. 16, p. 489.
15. Popov, K.I., Stojilković, E.R., Radmilović, V., and Pavlović, M.G., *Powder Technol.,* 1997, vol. 93, p. 55.
16. Yao, C.-Z., Liu, M., Zhang, P., He, X.-H., Li, G.-R., Zhao, W.-X., Liu, P., and Tong, Y.-X., *Electrochim. Acta,* 2008, vol. 54, p. 247.
17. Nikolić, N.D., Branković, G., and Lačnjevac, U.Č., *J. Solid State Electrochem.,* 2012, vol. 16, p. 2121.
18. Mostany, J., Parra, J., and Scharifker, B.R., *J. Appl. Electrochem.,* 1986, vol. 16, p. 333.
19. Owais, A., *World Metall.—Erzmet.,* 2012, vol. 65, p. 361.
20. Ehlers, C., König, U., Staikov, G., and Schultze, J.W., *Electrochim. Acta,* 2001, vol. 47, p. 379.
21. Rashkova, B., Guel, B., Pötzschke, R.T., Staikov, G., and Lorenz, W.J., *Electrochim. Acta,* 1998, vol. 43, p. 3021.
22. Cherevko, S., Xing, X., and Chung, C.-H., *Appl. Surf. Sci.,* 2011, vol. 257, p. 8054.
23. Nikolić, N.D., *Vaštag*, D.D., *Maksimović*, V.M., and *Branković*, G., *Trans. Nonferrous Met. Soc. China,* 2014, vol. 24, p. 884.
24. Carlos, I.A., Malaquias, M.A., Oizumi, M.M., and Matsuo, T.T., *J. Power Sources,* 2001, vol. 92, p. 56.
25. Ru, J., Bu, J., Wang, Z., Hua, Y., and Wang, D., *J. Appl. Electrochem.,* 2019, vol. 49, p. 369.
26. Ru, J., Hua, Y., Xu, C., Li, J., Li, Y., Wang, D., Qi, C., and Jie, Y., *Appl. Surf. Sci.,* 2015, vol. 335, p. 153.
27. Nikolić, N.D., Popov, K.I., Živković, P.M., and Branković, G., *J. Electroanal. Chem.,* 2013, vol. 691, p. 66.
28. Nikolić, N.D., Maksimović, V.M., Branković, G., Živković, P.M., and Pavlović, M.G., *J. Serb. Chem. Soc.,* 2013, vol. 78, p. 1387.
29. Nikolić, N.D., Popov, K.I., Ivanović, E.R., Branković, G., Stevanović, S.I., and Živković, P.M., *J. Electroanal. Chem.,* 2015, vol. 739, p. 137.
30. Nikolić, N.D., Vaštag, D.D., Živković, P.M., Jokić, B., and Branković, G., *Adv. Powder Technol.,* 2013, vol. 24, p. 674.
31. Ni, Y., Zhang, Y., and Hong, J., *CrystEngComm,* 2011, vol. 13, p. 934.
32. Carlos, I.A., Siqueira, J.L.P., Finazzi, G.A., and de Almeida, M.R.H., *J. Power Sources,* 2003, vol. 117, p. 179.
33. Kindy, H.M., Wahby, A.T., Koutnouyan, Z.Y., Salem, M.F., and Merchant, H.D., *Sci. Sintering,* 1980, vol. 12, p. 107.
34. Sun, Z., Zou, X.P., Cheng, J., Meng, X.M., Wei, C.L., Yang, G.Q., Lü, X.M., Feng, H.Y., and Yang, Y., *Adv. Mater. Res.,* 2010, vols. 123–125, p. 659.
35. Lü, X.M., Zou, X.P., Cheng, J., Ren, P.F., Meng, X.M., Yang, G.Q., Wei, C.L., and Sun, Z., *Adv. Mater. Res.,* 2010, vols. 123–125, p. 1279.
36. Zhitomirsky, I., Gal-Or, L., Kohn, A., and Hennicke, H.W., *J. Mater. Sci. Lett.,* 1995, vol. 14, p. 807.
37. Meng, L., Ustarroz, J., Newton, M.E., and Macpherson, J.V., *J. Phys. Chem. C,* 2017, vol. 121, p. 6835.
38. Sawatani, S., Ogawa, S., Yoshida, T., and Minoura, H., *Adv. Funct. Mater.,* 2005, vol. 15, p. 297.
39. Kwon, Y., Lee, H., and Lee, J., *Nanoscale,* 2011, vol. 3, p. 4984.
40. Cheng, J.I.N., Zou, X., Su, Y.I., Yang, G., and Lü, X., *Funct. Mater. Lett.,* 2009, vol. 02, p. 185.

41. Pan, J., Sun, Y., Li, W., Knight, J., and Manthiram, A., *Nat. Commun.,* 2013, vol. 4, article no. 2178.
42. Pan, J., Zhang, X., Sun, Y., Song, S., Li, W., and Wan, P., *Ind. Eng. Chem. Res.,* 2016, vol. 55, p. 2059.
43. Wang, Y.-y., Chai, L.-y., Chang, H., Peng, X.-y., and Shu, Y.-d., *Trans. Nonferrous Met. Soc. China,* 2009, vol. 19, p. 458.
44. Vijh, A.K. and Randin, J.P., *Surf. Technol.,* 1977, vol. 5, p. 257.
45. Nikolić, N.D., Maksimović, V.M., and Branković, G., *RSC Adv.,* 2013, vol. 3, p. 7466.
46. Pavlov, D. and Monahov, B., *J. Electrochem. Soc.,* 1996, vol. 143, p. 3616.
47. Pavlov, D., Balkanov, I., Halachev, T., and Rachev, P., *J. Electrochem. Soc.,* 1989, vol. 136, p. 3189.
48. Pavlov, D., *J. Electrochem. Soc.,* 1992, vol. 139, p. 3075.
49. Persson, K., *Materials Data on Pb2O (SG:224) by Materials Project,* 2016.
50. Yadav, V.S.K. and Purkait, M.K., *RSC Adv.,* 2015, vol. 5, p. 40414.
51. Easterday, C.C., Dedon, L.R., Zeller, M., and Oertel, C.M., *Cryst. Growth Des.,* 2014, vol. 14, p. 2048.
52. Veluchamy, P. and Minoura, H., *J. Mater. Sci. Lett.,* 1996, vol. 15, p. 1705.